

ORIGINAL ARTICLE

Multimodality Imaging Characteristics of the Common Renal Cell Carcinoma Subtypes: An Analysis of 544 Pathologically Proven Tumors

Winnie Fu¹, Guan Huang¹, Zaahir Moloo², Safwat Girgis³, Vimal H Patel¹, Gavin Low^{1,2}

Departments of ¹Radiology and Diagnostic Imaging and ³Pathology, University of Alberta Hospital, ²Faculty of Medicine and Dentistry, University of Alberta, Edmonton, Alberta, Canada

Address for correspondence:

Dr. Winnie Fu,
Department of Radiology and Diagnostic
Imaging, University of Alberta Hospital,
2A2.41 WMC, 8440-112 Street,
Edmonton, AB T6G 2B7, Canada.
E-mail: akaie_stm@hotmail.com



Received : 25-08-2016

Accepted : 21-11-2016

Published : 29-12-2016

ABSTRACT

Objectives: The objective of this study was to define the characteristic imaging appearances of the common renal cell carcinoma (RCC) subtypes. **Materials and Methods:** The Institutional Review Board approval was obtained for this HIPAA-compliant retrospective study, and informed consent was waived. 520 patients (336 men, 184 women; age range, 22–88 years) underwent preoperative cross-sectional imaging of 544 RCCs from 2008 to 2013. The imaging appearances of the RCCs and clinical information were reviewed. Data analysis was performed using parametric and nonparametric statistics, descriptive statistics, and receiver operating characteristic analysis. **Results:** The RCC subtypes showed significant differences ($P < 0.001$) in several imaging parameters such as tumor margins, tumor consistency, tumor homogeneity, the presence of a central stellate scar, T2 signal intensity, and the degree of tumor enhancement. Low T2 signal intensity on magnetic resonance imaging (MRI) allowed differentiation of papillary RCC from clear cell and chromophobe RCCs with 90.9% sensitivity and 93.1% specificity. A tumor-to-cortex ratio ≥ 1 on the corticomedullary phase had 98% specificity for clear cell RCC. **Conclusion:** The T2 signal intensity of the tumor on MRI and its degree of enhancement are useful imaging parameters for discriminating between the RCC subtypes while gross morphological findings offer additional value in RCC profiling.

Key words: Corticomedullary phase, multimodality imaging, renal cell carcinoma subtypes, T2 signal intensity, tumor-to-cortex ratio

Access this article online

Quick Response Code:



Website:

www.clinicalimagingscience.org

DOI:

10.4103/2156-7514.197026

This is an open access article distributed under the terms of the Creative Commons Attribution-NonCommercial-ShareAlike 3.0 License, which allows others to remix, tweak, and build upon the work non-commercially, as long as the author is credited and the new creations are licensed under the identical terms.

For reprints contact: reprints@medknow.com

How to cite this article: Fu W, Huang G, Moloo Z, Girgis S, Patel VH, Low G. Multimodality Imaging Characteristics of the Common Renal Cell Carcinoma Subtypes: An Analysis of 544 Pathologically Proven Tumors. J Clin Imaging Sci 2016;6:50. Available FREE in open access from: <http://www.clinicalimagingscience.org/text.asp?2016/6/1/50/197026>

INTRODUCTION

Renal cell carcinoma (RCC) accounts for 90% of all malignant renal neoplasms in adults.^[1-3] Disease progression is fatal in up to 40%, making RCC the most lethal of all urologic malignancies.^[4] 40% of RCCs are discovered incidentally on imaging examinations performed for nonurologic indications.^[5] The incidence of RCC has increased globally, in part due to greater utilization of cross-sectional imaging leading to improved tumor detection, and heightened public awareness of health-related issues including obesity and smoking.^[5-7]

RCCs are classified histologically into distinct subtypes, of which clear cell, papillary, and chromophobe tumors represent the majority. Broadly, clear cell tumors account for 70%, papillary tumors 10%–15%, and chromophobe tumors 5%–6%.^[1,3,8,9] Subtype differentiation is important as the various subtypes are associated with differing biologic behaviors and clinical outcomes.^[8-10] Clear cell RCCs have a comparatively poor prognosis, papillary RCCs have an intermediate prognosis, and chromophobe RCCs have the best prognosis of the three.^[8-10] Thus, RCC subtyping may impact clinical decision-making and have therapeutic implications for patients.^[11] Several reports have suggested that imaging can play a noninvasive role in subtype differentiation.^[3,8,9,12,13] Clear cell RCCs have a predilection toward tumor heterogeneity compared with other subtypes^[3,13] due to intratumoral hemorrhage, necrosis, or cyst formation and are typically hypervascular on postcontrast studies.^[13-17] Papillary RCCs (generally type 1) typically appear homogeneous and hypovascular on cross-sectional imaging.^[12,13] Some chromophobe RCCs exhibit a homogeneous consistency despite being a relatively large size.^[18] Spoke-wheel enhancement and a central stellate scar – imaging findings initially observed in oncocytomas have recently been recognized in chromophobe RCCs as well.^[19-21] Several studies evaluated the degree of RCC enhancement subjectively and quantitatively^[13,22-27] while others correlated magnetic resonance imaging (MRI) findings such as diffusion-weighted imaging (DWI) and apparent diffusion coefficient (ADC) values, with the RCC subtype.^[28-31] Thus, the objectives of this present study were: (1) to define the characteristic imaging appearances of the various RCC subtypes including quantifying the degree of tumor enhancement, (2) to integrate the imaging findings with relevant demographic and clinical parameters, and (3) to frame the results of this study in the context of the existing literature.

MATERIALS AND METHODS

The Ethics and Institutional Review Board approval was obtained, and informed consent waived for this retrospective study. The institution's pathology database was scanned for all surgically resected RCCs from January 2008 to December 2013. The search yielded a total of 706 patients. Of this, 520 patients with 544 RCCs were enrolled into the study based on the following selection criteria: (1) surgically proven RCCs of either clear cell, papillary, or chromophobe subtype and (2) availability of relevant preoperative cross-sectional imaging studies, including ultrasound (US), computed tomography (CT), and/or MRI, on the citywide picture archiving and communication system (PACS) system.

The following imaging parameters were documented in each RCC: Size, location, margins, lesion homogeneity, and consistency, presence or absence of septations or mural nodules, presence or absence of calcifications, intratumoral fat or central stellate scar, echogenicity on US, vascularity on Doppler, degree of enhancement on CT, phase of maximum enhancement on CT, signal characteristics on MRI, tumor stage, and presence or absence of tumor growth. In cases that included a four-phase CT examination (unenhanced phase, corticomedullary phase [CMP], nephrographic phase [NGP], and excretory phase [EXP]), the absolute enhancement ratio (AER) and tumor-to-cortex ratio (TCR) were derived as quantitative indices of tumor enhancement. The CT attenuation of the RCC was obtained by drawing the largest region of interest (ROI) that could be accommodated within the most enhancing portion of the tumor on each available phase while avoiding cystic and necrotic areas and partial volume effects from adjacent structures. The renal cortex ROI was placed over a section of the ipsilateral kidney that was not involved by the tumor or alternatively over the contralateral kidney if the tumor had completely replaced the involved kidney.

$$\text{AER of the tumor} = \frac{\text{CT attenuation(enhanced)} - \text{CT attenuation(unenhanced)}}{\text{CT attenuation(unenhanced)}}$$

$$\text{TCR} = \frac{\text{CT attenuation (tumor)}}{\text{CT attenuation (cortex)}}$$

The maximum AER and the phase in which this occurred were documented. The following MRI parameters were evaluated: T1 and T2 signal intensity, presence or absence of intratumoral fat, ADC value of the tumor, and ratio of tumor ADC to renal parenchyma ADC for b-value of 500 s/mm². An ROI ≥ 1 cm² was placed over the solid portion of the tumor

on the ADC map. To obtain the renal parenchyma ADC, an ROI of 1 cm² was placed over the uninvolved ipsilateral renal cortex, or alternatively, the contralateral cortex if the tumor completely involved the kidney.

The clinical information of all 520 patients was reviewed for the following clinical variables: Age at tumor discovery, gender, body mass index, and a past medical history of any of the following - hypertension, renal calculi, renal disease, renal transplant, previous cancer, a first-degree relative with kidney cancer, a predisposing genetic syndrome, nonsteroidal anti-inflammatory drug (NSAID) use, and smoking history.

Image interpretation

Two fellowship-trained board-certified abdominal radiologists (WF and GL) performed a consensus review of the tumor imaging features on all the cross-sectional imaging studies, including US, CT, and MRI retrospectively with prior knowledge of the clinical and laboratory information. The images were displayed in digital imaging and communications in medicine format on the PACS workstation (IMPAX 6.1, AGFA Healthcare) in the radiology department of our institution.

Imaging techniques

The imaging modalities performed and the protocols employed varied because cases were acquired from several hospitals within the city. The subtle variations in technique over the 7-year study period in this retrospective study may be a potential confounding factor. To minimize a potential bias from varying dynamic contrast-enhanced CT imaging protocols, we studied the maximum tumor enhancement ratio and TCR on CT rather than actual values of tumor enhancement to quantitatively assess tumor enhancement in the three postcontrast phases. The typical protocols at our institution were as follows:

- US examinations were performed using a 1–5 MHz curved array probe with the patient either in a supine or in an oblique lateral position. Short-axis and long-axis sectional images of the tumor were acquired in gray-scale and color Doppler modes
- CT examinations included a combination of the following: An unenhanced CT phase, a CMP at 25 s after contrast injection, an NGP at 80 s after contrast injection, and an EXP at 120 s after contrast injection. Multiplanar axial, coronal, and sagittal datasets were acquired. Standard CT parameters include a slice thickness of 2 mm, reconstruction interval of 2 mm, tube voltage of 120 kVp, and a tube current of 240 mAs. Typically, 100 ml of nonionic iodinated contrast media was administered intravenously at 4 mL/s by power injection

- MRI examinations were performed on 1.5-T clinical systems using a combination of unenhanced MR sequences and multiphasic contrast-enhanced MR sequences typically acquired at 25–30 s after contrast injection (CMP), 75–80 s after contrast injection (NGP), and 120–180 s after contrast injection (EXP). Standard unenhanced MR sequences included axial and/or coronal T1-weighted dual-echo in-and-out-of-phase sequences and axial and/or coronal turbo spin-echo T2-weighted sequences with or without fat suppression (FS). Dynamic postcontrast examinations were performed using a 3D FS T1-weighted sequence following intravenous administration of gadolinium (0.1–0.2 mL/kg) at a rate of 2–5 mL/s by power injection. The slice thickness per sequence was 4–6 mm.

Statistical analyses

Continuous variables including patient's age, tumor size, ADC values, maximum tumor enhancement ratio, and TCR on CT were expressed as mean ± standard deviation and categorical variables including patient's gender and clinical history, tumor multiplicity, location, sonographic features, MRI signal features, phase of maximum tumor enhancement on CT, interval growth, and staging were expressed as values and percentages. The study data – missing values excluded – were subjected to the following statistical tests, where appropriate:

- Chi-square test for categorical variables
- One-way ANOVA for continuous variables (*post hoc* analysis with a Bonferroni correction)
- Descriptive statistics (sensitivity, specificity, positive predictive value [PPV], and negative predictive value [NPV])
- Receiver operating characteristic (ROC) analysis.

All analyses were performed on commercially available statistical software (IBM SPSS Statistics, version 22, 2013, USA). $P < 0.05$ was considered statistically significant.

RESULTS

There were 520 patients (mean age – 60 years, age range – 22–88 years, 336 males and 184 females with a male to female ratio of 1.8) with 544 RCCs. 410 (78.8%) patients had 425 (78.1%) clear cell RCCs, 78 patients (15%) had 87 (16%) papillary RCCs, and 32 (6.2%) patients had 32 (5.9%) chromophobe RCCs.

Demographic and clinical characteristics

Data on patient demographics and clinical characteristics are included in Table 1. A strong male predilection was observed for all subtypes – with the papillary subtype

Table 1: Demographic and clinical characteristics of the renal cell carcinoma subtypes

	CC	P	C	P
Number of patients (%)	410/520 (78.8)	78/520 (15)	32/520 (6.2)	
Age (years)	60 ± 12	62 ± 11	57 ± 15	0.20
Age range	22-88	21-81	32-81	
Gender (% male)	255/410 (62.2)	62/78 (79.5 **)	19/32 (59.4)	0.01
Clinical information (%)				
Hypertension	188/410 (45.9)	36/78 (46.2)	13/32 (40.6)	0.84
Renal calculi	30/410 (7.3)	9/78 (11.5)	4/32 (12.5)	0.31
Renal disease	76/410 (18.5)	29/78 (37.2 **)	6/32 (18.8)	0.01
Transplant recipient	4/410 (1)	4/78 (5.1 **)	0/32 (0)	0.04
History of cancer	53/410 (12.9)	9/78 (11.5)	3/32 (9.4)	0.81
Family history of renal cancer	3/410 (0.7)	0/78 (0)	0/32 (0)	0.49
Predisposing genetic syndrome	1/410 (0.2)	0/78 (0)	0/32 (0)	0.79
Smoking history	133/410 (32.4)	16/78 (20.5)	7/32 (21.9)	0.06
BMI ≥ 25	79/410 (19.3)	10/78 (12.8)	1/32 (3.1 **)	0.04
NSAID usage	31/410 (7.6)	8/78 (10.3)	3/32 (9.4)	0.70
None of the above	103/410 (25.1)	20/78 (25.6)	12/32 (37.5)	0.31

**Data which are significantly different from that of the other groups. CC: Clear cell, P: Papillary, C: Chromophobe, BMI: Body mass index, NSAID: Nonsteroidal anti-inflammatory drug

showing a significantly greater proportion of males compared with the other subtypes. The papillary subtype had a significantly greater proportion of subjects with either preexisting renal disease or kidney transplants compared with the other subtypes. There were no significant differences between the subtypes for parameters such as age, history of hypertension, history of renal calculi, history of cancer, family history of renal cancer, a predisposing genetic syndrome, smoking history, NSAID use, or the proportion of subjects with none of the evaluable parameters.

Imaging characteristics

Data on the imaging characteristics of the tumor subtypes are included in Table 2. 425 tumors with clear cell subtype were evaluated by US, while 67 of those were evaluated by MRI and 387 of those were evaluated by CT. 87 tumors with papillary subtype were evaluated by US, while 11 of those were evaluated by MRI and 69 of those were evaluated by CT. 32 tumors with chromophobe subtype were evaluated by US, while 5 of those were evaluated by MRI and 31 of those were evaluated by CT. The chromophobe subtype had a significantly larger mean size compared with the papillary subtype [Figure 1]. The clear cell subtype had a significantly greater proportion of tumors that were poorly marginated and heterogeneous [Figure 2] compared with the other subtypes. Most papillary tumors were well marginated and homogeneous [Figure 3a]. While most chromophobe tumors were well marginated, this subtype had an equal number of homogeneous and heterogeneous lesions. The tumor consistency was most frequently completely solid for all subtypes – nevertheless, the clear cell subtype had a significantly lower proportion of tumors with a completely solid consistency and a significantly higher proportion of tumors with a mixed consistency (solid >cystic) compared with the other subtypes. A central stellate scar appeared

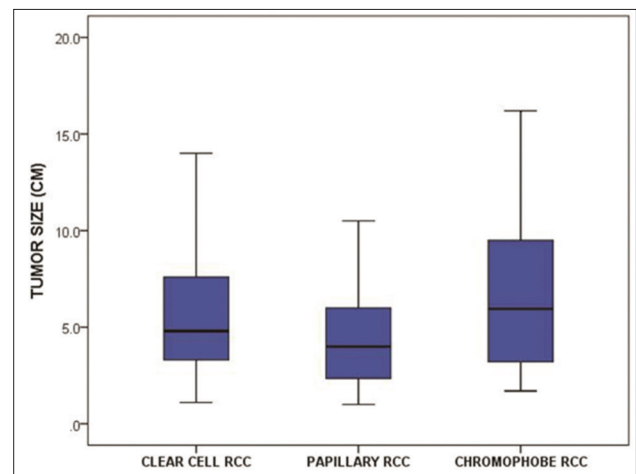


Figure 1: Boxplots show the tumor size of the renal cell carcinoma subtypes.

to be an exclusive feature of the chromophobe subtype. It was visualized on CT and confirmed on histology in 6 of 32 (18.8%) chromophobe tumors – no clear cell or papillary tumors showed a central stellate scar [Figure 4]. On US, hypoechoic, isoechoic, and hyperechoic tumors were found in all subtypes. However, the clear cell subtype had a significantly lower proportion of tumors that were hypoechoic and a significantly higher proportion of tumors that were hyperechoic compared with the other subtypes. The papillary subtype had a significantly greater proportion of tumors that were avascular on Doppler US compared with the others – most clear cell and chromophobe tumors showed vascularity. On MRI, the majority of papillary tumors showed low T2 signal intensity [Figure 3a]. This finding was a significant discriminator for the papillary subtype compared with the other subtypes. The majority of clear cell tumors [Figure 2] and 3 of 5 chromophobe tumors on MRI showed high T2 signal intensity. However, T2 isointensity with the renal cortex was found in a significantly greater proportion of chromophobe tumors (2 of 5, 40%) compared

Table 2: Imaging characteristics of the renal cell carcinoma subtypes

	CC	P	C	P
Number of tumors (%)	425/544 (78.1)	87/544 (16)	32/544 (5.9)	
Multiplicity (%)				
Single	397/410 (96.8)	73/78 (93.6)	32/32 (100)	0.14
Multiple	13/410 (3.2)	5/78 (6.4)	0/32 (0)	
Location (%)				
Right	184/412 (44.7)	47/83 (56.6)	11/32 (34.4)	0.17
Left	215/412 (52.2)	33/83 (39.8)	21/32 (65.6)	
Bilateral	12/412 (2.9)	3/83 (3.6)	0/32 (0)	
Transplant	1/412 (0.2)	0/83 (0)	0/32 (0)	
Size (cm)	5.8±3.4	5±3.9**	7±4.5**	0.02 (overall) P versus C; P=0.02*
Margins (%)				
Well marginated	195/425 (45.9**)	76/87 (87.4)	27/32 (84.4)	<0.001
Poorly marginated	230/425 (54.1**)	11/87 (12.6)	5/32 (15.6)	
Homogeneity (%)				
Homogeneous	30/425 (7.1**)	59/87 (67.8)	16/32 (50)	<0.001
Heterogeneous	395/425 (92.9**)	28/87 (32.2)	16/32 (50)	
Consistency (%)				
Completely solid	195/425 (45.9**)	67/87 (77)	25/32 (78.1)	<0.001
Completely cystic	29/425 (6.8)	5/87 (5.7)	0/32 (0)	
Mixed with solid > cystic	179/425 (42.1**)	8/87 (9.2)	6/32 (18.8)	
Mixed with cystic > solid	22/425 (5.2)	7/87 (8.1)	1/32 (3.1)	
Central stellate scar (%)	0/419 (0)	0/86 (0)	6/32 (18.8**)	<0.001
Calcifications (%)	81/425 (19.1)	15/87 (17.2)	11/32 (34.4)	0.09
Intratumoral fat (%)				
Macroscopic fat on CT ± MRI	2/419 (0.5)	2/86 (2.3)	0/32 (0)	0.25
Microscopic fat on MRI	4/67 (6)	0/11 (0)	0/5 (0)	0.44
Septations, if completely cystic or cystic >solid (%)	33/51 (64.7)	4/12 (33.3)	0/1 (0)	0.36
Mural nodules (%)	5/51 (9.8)	1/12 (8.3)	0/1 (0)	0.89
Echogenicity (%)				
Anechoic	14/232 (6)	1/42 (2.4)	0/11 (0)	<0.001
Hypoechoic	38/232 (16.4**)	19/42 (45.2)	5/11 (45.4)	
Isoechoic	46/232 (19.8)	9/42 (21.4)	3/11 (27.3)	
Hyperechoic	134/232 (57.8**)	13/42 (31)	3/11 (27.3)	
Doppler ultrasound (%)				
Avascular	25/223 (11.2)	21/41 (51.2**)	3/11 (27.3)	<0.001
Vascular	198/223 (88.8)	20/41 (48.8**)	8/11 (72.7)	
MRI signal (%)				
Low T1 and T2	4/67 (6)	5/11 (45.5**)	0/5 (0)	<0.001
Low T1, high T2	51/67 (76.1)	1/11 (9**)	3/5 (60)	
High T1, low T2	1/67 (1.5)	5/11 (45.5**)	0/5 (0)	
High T1 and T2	9/67 (13.4)	0/11 (0)	0/5 (0)	
Low T1, isoechoic T2	2/67 (3)	0/11 (0)	2/5 (40**)	
MRI signal subanalysis (%)				
Low T2	5/67 (7.4)	10/11 (91**)	0/5 (0)	<0.001
High T2	60/67 (89.6)	1/11 (9**)	3/5 (60)	
Isoechoic T2	2/67 (2.9)	0/11 (0)	2/5 (40**)	
ADC				
Tumor	1836±511	1451±755	N/A	0.33
Tumor/kidney	0.8±0.2	0.8±0.5	N/A	0.74
Tumor enhancement on CT (%)				
Appreciable (≥15 HU)	381/387 (98.4)	51/69 (73.9**)	31/31 (100)	<0.001
Not appreciable (<15 HU)	6/387 (1.6)	18/69 (26.1**)	0/31 (0)	
Maximum tumor enhancement ratio on CT:	3.2±1.7**	1.0±0.6	1.3±0.4	<0.001 (overall) CC versus P; P<0.001* CC versus C; P=0.003*
Phase of maximum tumor enhancement on CT (%)				
Corticomedullary	81/99 (81.8**)	1/14 (7.1)	3/8 (37.5)	<0.001
Nephrographic	17/99 (17.2**)	13/14 (92.9)	5/8 (62.5)	
Excretory	1/99 (1)	0/14 (0)	0/8 (0)	
TCR				
Unenhanced	1.2±0.7	1.1±0.4	1.2±0.3	0.79

Contd...

Table 2: Contd...

	CC	P	C	P
Corticomedullary	0.9 ± 0.3**	0.4 ± 0.2	0.5 ± 0.1	<0.001 (overall) CC versus P/CC versus C; P < 0.001 *
Nephrographic	0.7 ± 0.1**	0.5 ± 0.1	0.5 ± 0.2	<0.001 (overall) CC versus P/CC versus C; P < 0.001 *
Excretory	0.7 ± 0.2**	0.6 ± 0.1	0.5 ± 0.1	<0.001 (overall) CC versus P/CC versus C; P = 0.01 *
Interval growth (%)				
Stable	28/47 (59.6)	6/11 (54.5)	N/A	0.76
Progressive (≥20% increase)	19/47 (40.4)	5/11 (45.5)	N/A	
Stage (AJCC), (%)				
I	260/425 (61.2)	64/87 (73.6**)	16/32 (50)	<0.001
II	38/425 (8.9)	6/87 (6.9)	11/32 (34.4**)	
III	76/425 (17.9)	12/87 (13.8)	4/32 (12.5)	
IV	51/425 (12)	5/87 (5.7)	1/32 (3.1)	
Extent of involvement (%)				
Confined to kidney	298/425 (70.1)	70/87 (80.5)	27/32 (84.3)	0.27
Locally invasive	20/425 (4.7)	3/87 (3.4)	2/32 (6.3)	
Vascular involvement	55/425 (12.9)	8/87 (9.2)	2/32 (6.3)	
Organ metastases	16/425 (3.8)	4/87 (4.6)	0/32 (0)	
Lymph node involvement	36/425 (8.5)	2/87 (2.3)	1/32 (3.1)	

**Data which are significantly different from that of the other groups; *Post hoc analysis with a Bonferroni correction. N/A: Not applicable, CC: Clear cell, P: Papillary, C: Chromophobe, CT: Computed tomography, MRI: Magnetic resonance imaging, ADC: Apparent diffusion coefficient, TCR: Tumor-to-cortex ratio, AJCC: American Joint Committee on Cancer

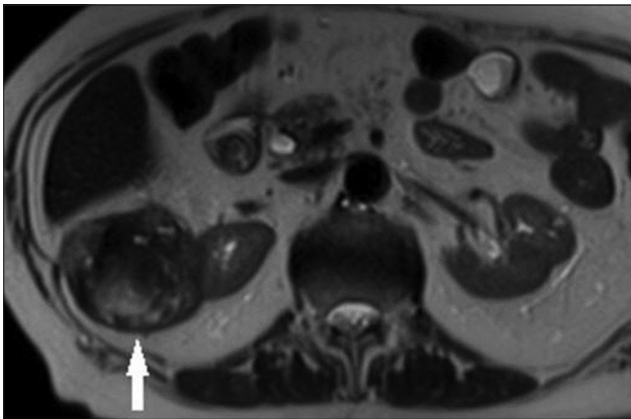


Figure 2: A 79-year-old female with a pathologically proven clear cell renal cell carcinoma in the right kidney on an axial T2-weighted magnetic resonance image. The exophytic tumor (arrow) has a heterogeneous internal consistency, including foci of high signal intensity.

with cell clear (2 of 67, 2.9%) and papillary (0 of 11, 0%) tumors. Table 3 illustrates the diagnostic performance of MRI for detecting papillary and chromophobe tumors based on the T2 signal intensity.

Most RCCs irrespective of subtype showed tumor enhancement, in particular, clear cell tumors [Figure 5]. However, 18 of 69 (26.1%) papillary tumors – a statistically significant finding – did not show appreciable enhancement on CT (<15 HU difference in tumor density between enhanced and unenhanced CT images) [Figure 3b]. The maximum AER on CT was significantly greater for the clear cell subtype compared with the other subtypes [Figure 6]. The clear cell subtype had a significantly greater proportion

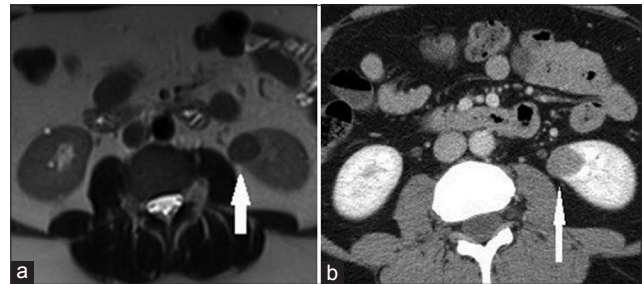


Figure 3: (a) A 62-year-old male with a pathologically proven papillary renal cell carcinoma in the left kidney on an axial T2-weighted magnetic resonance image. The well-circumscribed solid tumor (arrow) shows homogeneous low T2 signal intensity. (b) A 62-year-old male with a pathologically proven papillary renal cell carcinoma in the left kidney on an axial contrast-enhanced computed tomography image during the nephrographic phase. The well-circumscribed hypovascular solid tumor (arrow) has a homogeneous internal consistency.

of tumors that exhibited maximum enhancement on the CMP while the papillary and chromophobe subtypes had a significantly greater proportion of tumors that exhibited maximum enhancement on the NGP. The phase of maximum AER on CT was most frequently the CMP followed by the NGP and EXP for clear cell tumors and the NGP followed by the CMP and EXP for papillary and chromophobe tumors. The TCR for the clear cell subtype on all enhanced CT phases was significantly greater compared with that of the other subtypes. The diagnostic performance of TCR for differentiating the clear cell subtype from the other subtypes is illustrated in Figure 7 and Table 4. The CMP showed the best performance – a CMP TCR ≥ 1 had a sensitivity of 31.9% (95% confidence interval [CI]: 26.1%–38.3%), specificity of 98% (95% CI:

Table 3: Diagnostic performance of magnetic resonance imaging for papillary and chromophobe renal cell carcinomas based on T2 signal intensity

	Sensitivity + 95% CI	Specificity + 95% CI	PPV + 95% CI	NPV + 95% CI
T2 low signal for papillary RCC (%)	90.9 (58.7-98.5)	93.1 (84.5-97.7)	66.7 (38.4-88.1)	98.5 (92.1-99.8)
T2 isoechoic signal for chromophobe RCC (%)	40 (6.5-84.6)	97.4 (91-99.6)	50 (8.3-91.7)	96.2 (89.3-99.2)

CI: Confidence interval, PPV: Positive predictive value, NPV: Negative predictive value, RCC: Renal cell carcinomas



Figure 4: A 54-year-old female with a pathologically proven chromophobe renal cell carcinoma in the right kidney on an axial contrast-enhanced computed tomography image during the nephrographic phase. The large well-circumscribed solid tumor (arrow) shows a hypoattenuating central stellate scar. A simple cyst is incidentally noted in the left kidney.



Figure 5: A 42-year-old female with a pathologically proven clear cell renal cell carcinoma in the right kidney on an axial contrast-enhanced computed tomography image during the corticomedullary phase. The complex cystic tumor has a hypervascular solid mural nodule (arrow).

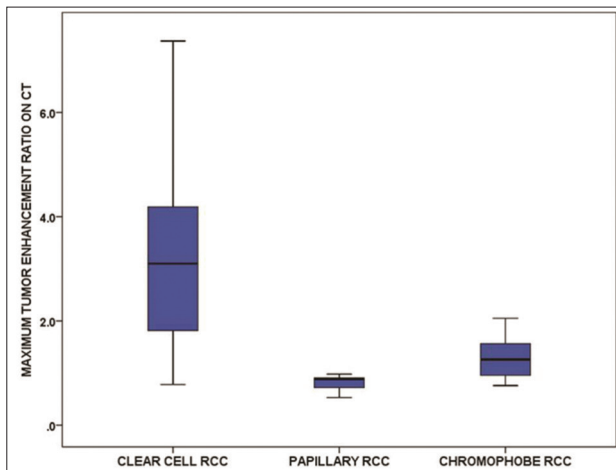


Figure 6: Boxplots show the maximum tumor enhancement ratio on computed tomography of the renal cell carcinoma subtypes.

89.6%–100%), PPV of 98.3% (95% CI: 94.4%–99.7%), and NPV of 28.7% (24.4%–33.4%) for the clear cell subtype.

The most common stage for all subtypes was stage 1 – with the papillary subtype showing a significantly greater proportion of stage 1 tumors compared with the other subtypes. For stage 2 tumors, there was a significantly greater proportion of chromophobe tumors compared with the other subtypes. The proportion of stage 3 and 4 tumors was not significantly different between the subtypes. Despite the malignant etiology,

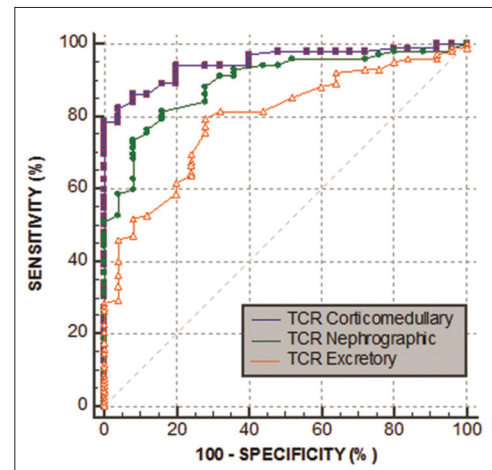


Figure 7: Receiver operating characteristic analysis of the diagnostic performance of tumor-to-cortex ratio for differentiating the clear cell subtype from the other renal cell carcinoma subtypes on various computed tomography phases.

over half of clear cell and papillary tumors were stable over a minimum period of 3 months. Furthermore, there were no significant differences in the proportion of stable versus progressive tumors between the two subtypes. The chromophobe subtype was not evaluated for this variable as none of the chromophobe tumors had a presurgical follow-up examination of at least 3 months. Finally, there were no significant differences between the subtypes for the following parameters – single or multiple tumors, tumor location, calcifications, intratumoral fat,

Table 4: Receiver operating characteristic analysis of the diagnostic performance of tumor-to-cortex ratio for differentiating the clear cell subtype from other renal cell carcinomas subtypes on various computed tomography phases

TCR	A _z	95% CI	P
Corticomedullary phase	0.93	0.89-0.95	<0.0001
Nephrographic phase	0.83	0.79-0.87	<0.0001
Excretory phase	0.75	0.69-0.80	<0.0001

TCR: Tumor-to-cortex ratio, A_z: Area under the receiver operating characteristic curve, CI: Confidence interval

septations, mural nodules, ADC value, or the extent of tumor involvement.

DISCUSSION

Our study found several significant differences between the RCCs subtypes on imaging. This included gross morphologic findings such as the tumor margins (well marginated vs. poorly marginated), tumor consistency (completely solid vs. completely cystic vs. mixed solid and cystic), and tumor homogeneity (homogeneous vs. heterogeneous). Most nonclear cell RCCs were well marginated (>84%) and completely solid ($\geq 77\%$) while over half of clear cell RCCs were poorly marginated and under half were completely solid. Over 92% of clear cell RCCs were heterogeneous while over 67% of papillary RCC were homogeneous. Our findings are consistent with the previous reports.^[13,15,16,18,32] Among RCCs, a central stellate scar appeared to be an exclusive feature of the chromophobe subtype although it may also be found in oncocytoma.^[19-21] All cases involving a central stellate scar on imaging were confirmed histologically.

The tumor signal intensity on T2-weighted MR images was a helpful subtype discriminator. 91% of papillary RCCs showed low T2 signal while over 89% of clear cell RCCs showed high T2 signal. This is consistent with the previous reports.^[14,17,32,33]

Several studies found that the RCC subtypes can be differentiated by the tumor enhancement.^[13,15,26,27,32,34] We found that a CMP TCR ≥ 1 had 98% specificity for differentiating clear cell from nonclear cell subtypes. Quantitative evaluation of tumor enhancement by Kim et al., and Jinzaki et al., yielded similar findings.^[13,35] Compared with their studies, ours included a larger number of RCCs. Several other studies found that clear cell RCCs showed greater enhancement than nonclear cell RCCs but those studies did not evaluate tumor enhancement quantitatively.^[22-25] Avid enhancement in clear cell RCCs is attributed to its rich vascular network and alveolar microarchitecture.^[22] Consistent with Young et al., we found that the maximum enhancement for clear cell RCCs was on the CMP and for nonclear cell RCCs on the NGP.^[27] None

of the nonclear cell RCCs and only 1 of 425 clear cell RCCs showed maximum enhancement on the EXP.

Kim et al., found that calcifications were more common in papillary (32%) and chromophobe (38%) RCCs compared with clear cell (11%) RCCs.^[13] The ADC value on DWI has been investigated^[15,28-31] with Wang et al., and Taouli et al., suggesting a higher mean ADC value for clear cell RCCs compared with nonclear cell subtypes although Sandrasegaran et al., found no significant differences between the two. ADC comparisons between studies are made difficult by scanner variability and differences in MR acquisition parameters. Our study did not find any significant difference between subtypes for calcifications or ADC value, or parameters such as multiplicity, tumor location, intratumoral fat, septations, mural nodules, or the extent of tumor involvement. In terms of clinical characteristics, we found that a significantly higher proportion of patients with papillary RCCs had a history of renal disease or renal transplants. This is consistent with the previous reports.^[36,37]

Over half of clear cell and papillary RCCs were stable over a minimum 3-month period. This finding confirms that RCCs can show slow growth as suggested by others.^[38] It is important, therefore, that radiologists are aware that interval stability in a renal mass does not necessarily equate to a benign etiology. More than half of clear cell RCCs were hyperechoic on US. Thus, a hyperechoic renal mass cannot be assumed to be an angiomyolipoma and such cases may require further assessment by CT/MRI.

The RCC subtypes have been shown to discriminate noninvasively on imaging based on a combination of parameters such as T2 signal intensity, the degree of tumor enhancement, and gross morphological findings. This has implications for patient care given that the different RCC subtypes are associated with different biologic behaviors, prognosis, and response to therapy. However, tissue diagnosis is generally required to determine if a lesion is benign or malignant.

Our study has several limitations. The number of papillary (87) and chromophobe (32) RCCs was relatively small due to their low incidence in clinical practice. There was a selection bias toward lower stage tumors given that most RCCs in our pathologic database were surgical cases performed for curative intent. The most common stage in all subtypes was stage 1, and the frequency of tumor invasion in our study was lower than in previous reports.^[1,2] To maximize the number of eligible cases, we reviewed all available imaging studies, including those from outside institutions. In this retrospective study which included RCCs scanned over a 7-year period, we noticed some technical

variability between studies as a result of scanner differences and nonuniform imaging protocols. Therefore, our criterion of tumor enhancement was applied only to those cases from outside institutions where the imaging parameters were similar to those performed at our institution.

CONCLUSION

The T2 signal intensity of the tumor on MRI and its degree of enhancement are the most useful imaging parameters for discriminating between the RCC subtypes, and gross morphological findings such as the tumor margins, tumor consistency, tumor homogeneity, and a central stellate scar offer additional value in RCC profiling.

Financial support and sponsorship

Nil.

Conflicts of interest

There are no conflicts of interest.

REFERENCES

- Bonsib SM. Risk and prognosis in renal neoplasms. A pathologist's prospective. *Urol Clin North Am* 1999;26:643-60, viii.
- McClellan BL, Deyoe LA. The imaging evaluation of renal cell carcinoma: Diagnosis and staging. *Radiol Clin North Am* 1994;32:55-69.
- Sheir KZ, El-Azab M, Mosbah A, El-Baz M, Shaaban AA. Differentiation of renal cell carcinoma subtypes by multislice computerized tomography. *J Urol* 2005;174:451-5.
- Jemal A, Murray T, Ward E, Samuels A, Tiwari RC, Ghafoor A, et al. Cancer statistics, 2005. *CA Cancer J Clin* 2005;55:10-30.
- Leslie JA, Prihoda T, Thompson IM. Serendipitous renal cell carcinoma in the post-CT era: Continued evidence in improved outcomes. *Urol Oncol* 2003;21:39-44.
- Frank I, Blute ML, Cheville JC, Lohse CM, Weaver AL, Zincke H. Solid renal tumors: An analysis of pathological features related to tumor size. *J Urol* 2003;170(6 Pt 1):2217-20.
- Chow WH, Devesa SS, Warren JL, Fraumeni JF Jr. Rising incidence of renal cell cancer in the United States. *JAMA* 1999;281:1628-31.
- Mydlo JH, Weinstein R, Misseri R, Axiotis C, Thelmo W. Radiologic, pathologic and molecular attributes of two types of papillary renal adenocarcinomas. *Scand J Urol Nephrol* 2001;35:262-9.
- Pignot G, Elie C, Conquy S, Vieillefond A, Flam T, Zerbib M, et al. Survival analysis of 130 patients with papillary renal cell carcinoma: Prognostic utility of type 1 and type 2 subclassification. *Urology* 2007;69:230-5.
- Leroy X, Zini L, Leteurtre E, Zerimech F, Porchet N, Aubert JP, et al. Morphologic subtyping of papillary renal cell carcinoma: Correlation with prognosis and differential expression of MUC1 between the two subtypes. *Mod Pathol* 2002;15:1126-30.
- Gudbjartsson T, Hardarson S, Petursdottir V, Thoroddsen A, Magnusson J, Einarsson GV. Histological subtyping and nuclear grading of renal cell carcinoma and their implications for survival: A retrospective nation-wide study of 629 patients. *Eur Urol* 2005;48:593-600.
- Herts BR, Coll DM, Novick AC, Obuchowski N, Linnell G, Wirth SL, et al. Enhancement characteristics of papillary renal neoplasms revealed on triphasic helical CT of the kidneys. *AJR Am J Roentgenol* 2002;178:367-72.
- Kim JK, Kim TK, Ahn HJ, Kim CS, Kim KR, Cho KS. Differentiation of subtypes of renal cell carcinoma on helical CT scans. *AJR Am J Roentgenol* 2002;178:1499-506.
- Shinmoto H, Yuasa Y, Tanimoto A, Narimatsu Y, Jinzaki M, Hiramatsu K, et al. Small renal cell carcinoma: MRI with pathologic correlation. *J Magn Reson Imaging* 1998;8:690-4.
- Zhang J, Tehrani YM, Wang L, Ishill NM, Schwartz LH, Hricak H. Renal masses: Characterization with diffusion-weighted MR imaging – A preliminary experience. *Radiology* 2008;247:458-64.
- Prasad SR, Humphrey PA, Catena JR, Narra VR, Srigley JR, Cortez AD, et al. Common and uncommon histologic subtypes of renal cell carcinoma: Imaging spectrum with pathologic correlation. *Radiographics* 2006;26:1795-806.
- Yoshimitsu K, Irie H, Tajima T, Nishie A, Asayama Y, Hirakawa M, et al. MR imaging of renal cell carcinoma: Its role in determining cell type. *Radiat Med* 2004;22:371-6.
- Mugiya S, Nagata M, Ozono S, Ito T, Maruyama S, Hadano S, et al. Ultrasonographic features of chromophobe cell renal carcinoma. *Hinyokika Kyo* 2004;50:865-8.
- Ren A, Cai F, Shang YN, Ma ES, Huang ZG, Wang W, et al. Differentiation of renal oncocytoma and renal clear cell carcinoma using relative CT enhancement ratio. *Chin Med J (Engl)* 2015;128:175-9.
- Rosenkrantz AB, Hindman N, Fitzgerald EF, Niver BE, Melamed J, Babb JS. MRI features of renal oncocytoma and chromophobe renal cell carcinoma. *AJR Am J Roentgenol* 2010;195:W421-7.
- Wu J, Zhu Q, Zhu W, Chen W, Wang S. Comparative study of CT appearances in renal oncocytoma and chromophobe renal cell carcinoma. *Acta Radiol* 2016;57:500-6.
- Fujimoto H, Wakao F, Moriyama N, Tobisu K, Sakamoto M, Kakizoe T. Alveolar architecture of clear cell renal carcinomas (<or = 5.0 cm) show high attenuation on dynamic CT scanning. *Jpn J Clin Oncol* 1999;29:198-203.
- Wildberger JE, Adam G, Boeckmann W, Münchau A, Brauers A, Günther RW, et al. Computed tomography characterization of renal cell tumors in correlation with histopathology. *Invest Radiol* 1997;32:596-601.
- Sheth S, Scatarige JC, Horton KM, Corl FM, Fishman EK. Current concepts in the diagnosis and management of renal cell carcinoma: Role of multidetector ct and three-dimensional CT. *Radiographics* 2001;21:S237-54.
- Garant M, Bonaldi VM, Taourel P, Pinsky MF, Bret PM. Enhancement patterns of renal masses during multiphase helical CT acquisitions. *Abdom Imaging* 1998;23:431-6.
- Sun MR, Ngo L, Genega EM, Atkins MB, Finn ME, Rofsky NM, et al. Renal cell carcinoma: Dynamic contrast-enhanced MR imaging for differentiation of tumor subtypes – Correlation with pathologic findings. *Radiology* 2009;250:793-802.
- Young JR, Margolis D, Sauk S, Pantuck AJ, Sayre J, Raman SS. Clear cell renal cell carcinoma: Discrimination from other renal cell carcinoma subtypes and oncocytoma at multiphasic multidetector CT. *Radiology* 2013;267:444-53.
- Zhang J, Pedrosa I, Rofsky NM. MR techniques for renal imaging. *Radiol Clin North Am* 2003;41:877-907.
- Taouli B, Thakur RK, Mannelli L, Babb JS, Kim S, Hecht EM, et al. Renal lesions: Characterization with diffusion-weighted imaging versus contrast-enhanced MR imaging. *Radiology* 2009;251:398-407.
- Wang H, Cheng L, Zhang X, Wang D, Guo A, Gao Y, et al. Renal cell carcinoma: Diffusion-weighted MR imaging for subtype differentiation at 3.0 T. *Radiology* 2010;257:135-43.
- Sandrasegaran K, Sundaram CP, Ramaswamy R, Akisik FM, Rydberg MP, Lin C, et al. Usefulness of diffusion-weighted imaging in the evaluation of renal masses. *AJR Am J Roentgenol* 2010;194:438-45.
- Pedrosa I, Sun MR, Spencer M, Genega EM, Olumi AF, Dewolf WC,

- et al. MR imaging of renal masses: Correlation with findings at surgery and pathologic analysis. *Radiographics* 2008;28:985-1003.
33. Oliva MR, Glickman JN, Zou KH, Teo SY, Mortelé KJ, Rocha MS, et al. Renal cell carcinoma: t1 and t2 signal intensity characteristics of papillary and clear cell types correlated with pathology. *AJR Am J Roentgenol* 2009;192:1524-30.
 34. Ruppert-Kohlmayr AJ, Uggowitz M, Meissnitzer T, Ruppert G. Differentiation of renal clear cell carcinoma and renal papillary carcinoma using quantitative CT enhancement parameters. *AJR Am J Roentgenol* 2004;183:1387-91.
 35. Jinzaki M, Tanimoto A, Mukai M, Ikeda E, Kobayashi S, Yuasa Y, et al. Double-phase helical CT of small renal parenchymal neoplasms: correlation with pathologic findings and tumor angiogenesis. *J Comput Assist Tomogr* 2000;24:835-42.
 36. Breda A, Lucarelli G, Rodriguez-Faba O, Guirado L, Facundo C, Bettocchi C, et al. Clinical and pathological outcomes of renal cell carcinoma (RCC) in native kidneys of patients with end-stage renal disease: A long-term comparative retrospective study with RCC diagnosed in the general population. *World J Urol* 2015;33:1-7.
 37. Woldu SL, Weinberg AC, RoyChoudhury A, Chase H, Kalloo SD, McKiernan JM, et al. Renal insufficiency is associated with an increased risk of papillary renal cell carcinoma histology. *Int Urol Nephrol* 2014;46:2127-32.
 38. Jhaveri K, Gupta P, Elmi A, Flor L, Moshonov H, Evans A, et al. Cystic renal cell carcinomas: Do they grow, metastasize, or recur? *AJR Am J Roentgenol* 2013;201:W292-6.